

Article

Numerical Simulation on Thermoelectric Cooling of Core Power Devices in Air Conditioning

Jiang Wang [†], Kai Hu [†], Kechen Tang, Yubing Xing, Yani Xiao, Yutian Liu, Yonggao Yan ^{*} and Dongwang Yang ^{*}

State Key Laboratory of Advanced Technology for Materials Synthesis and Processing, Wuhan University of Technology, Wuhan 430070, China; 303555@whut.edu.cn (J.W.); hk2020@whut.edu.cn (K.H.); tangkechen@whut.edu.cn (K.T.); xingyubing@whut.edu.cn (Y.X.); 303587@whut.edu.cn (Y.X.); liuyutian@whut.edu.cn (Y.L.)

^{*} Correspondence: yanyonggao@whut.edu.cn (Y.Y.); ydongwang@whut.edu.cn (D.Y.)

[†] These authors contributed equally to this work.

Abstract: Air conditioning has become a necessity in people's daily life. The performance of the compressor determines the energy efficiency ratio of this electrical equipment, but the heat generated during the operation of its internal core power components will greatly limit its performance release, so it is urgent to carry out research on the heat dissipation of power devices. In this work, we explore the application of thermoelectric coolers (TECs) in the field of power device heat dissipation through finite element simulation. First, we geometrically modeled the structure and typical operating conditions of core power devices in air conditioners. We compared the temperature fields in air-cooling and TEC active cooling modes for high-power-consumption power devices in a 319 K operating environment. The simulation results show that in the single air-cooling mode, the maximum temperature of the 173.8 W power device reached 394.4 K, and the average temperature reached 373.9 K, which exceeds its rated operating temperature of 368.1 K. However, the maximum and average temperature of the power device dropped to 331.8 K and 326.5 K, respectively, at an operating current of 7.5 A after adding TECs, which indicates that TEC active cooling has a significant effect on the temperature control of the power device. Furthermore, we studied the effect of the TEC working current on the temperature control effect of power devices to better understand the reliability of the TECs. The results show that TECs have a minimum working current of 5 A, which means it has no significant cooling effect when the working current is less than 5 A, and when increasing the current to 10 A, the average temperature of the power device can be reduced to 292.9 K. This study provides a meaningful exploration of the application of TECs in chip temperature control and heat dissipation, providing a new solution for chip thermal management and accurate temperature control.

Keywords: thermoelectric cooler; finite element simulation; power device; air conditioner; thermal management



Citation: Wang, J.; Hu, K.; Tang, K.; Xing, Y.; Xiao, Y.; Liu, Y.; Yan, Y.; Yang, D. Numerical Simulation on Thermoelectric Cooling of Core Power Devices in Air Conditioning. *Appl. Sci.* **2023**, *13*, 7274. <https://doi.org/10.3390/app13127274>

Academic Editors: Norhisam Bin Misron and Chockalingam Aravind Vaithilingam

Received: 26 May 2023
Revised: 17 June 2023
Accepted: 17 June 2023
Published: 19 June 2023



Copyright: © 2023 by the authors. Licensee MDPI, Basel, Switzerland. This article is an open access article distributed under the terms and conditions of the Creative Commons Attribution (CC BY) license (<https://creativecommons.org/licenses/by/4.0/>).

1. Introduction

In modern computer systems, the performance and integration of circuits continue to improve, which is one of the key factors driving the development of computer technology. However, this progress also brings a serious problem—the thermal management problem of the chip. With the development of Moore's Law, the number of transistors on an integrated circuit increases exponentially, leading to a corresponding exponential increase in heat generation per unit area [1–3]. When the chip's operating temperature exceeds the maximum rated temperature, it will cause irreversible damage to its structure [4]. To protect itself, when the chip overheats, it will reduce its processing frequency to reduce heat generation [5–7]. However, at the same time, the chip's frequency reduction also limits its performance release, and its thermal management problem gradually becomes the bottleneck that restricts its performance [8–12].

Early on, in order to control the temperature of the chip to maximize its performance, huge heat-sink fins [13–16] and cooling fans [17–19] were needed to take away the heat of the chip. However, these traditional heat dissipation solutions have the disadvantages of large volume and noise, making them difficult to apply to many precision instruments and electronic equipment. With the development of new heat dissipation technology, solutions have emerged such as water cooling [20] and liquid metal [21,22], as well as other phase change heat dissipation materials [23–27]. For example, a method that conducts heat from the chip to a thermal medium with a high specific heat capacity through heat pipes can take away the heat and ensure efficient temperature control of the chip [28–31]. Compared with traditional heat dissipation solutions, this method has the advantages of high efficiency, energy-saving, and environmental protection, and simultaneously introducing fluid media brings new risks to the system’s reliability, while volume problems remain unsolved [32]. With the increasing integration of electronic products, it is becoming difficult to meet the volume requirements of existing thermal technologies [33,34]. Therefore, there is an urgent need to research and explore a heat dissipation technology that can not only ensure the heat dissipation effect of the chip but also further reduce the volume and weight of electronic products, thereby improving the user experience and portability.

Thermoelectric cooling (TEC) is based on the semiconductor’s Peltier effect to achieve direct conversion from electricity to a temperature difference [35–38]. Its principle for refrigeration is shown in Figure 1. Compared to traditional compression refrigeration and phase change absorption refrigeration, thermoelectric refrigeration has a structure that lacks transmission parts, making it more reliable, stable, and with a longer lifespan. Additionally, it requires no maintenance and is noiseless [30,39–41]. The modularity, miniaturization [41–44], and efficiency of TEC devices fit well with the development of chips, which has a good prospect of application in the field of heat dissipation and temperature control of chips [45,46]. Some researchers have carried out corresponding research in this area. Moazzez et al. used ANSYS CFX software to simulate the air-cooling capacity of thermoelectric cooling devices under different conditions to develop the vehicle air conditioning refrigeration system [45]. Chen et al. systematically summarized the research progress of the most advanced on-chip thermoelectric cooling devices, and pointed out the development prospects of the design, performance, and application of these cooling devices [44]. Saleh used TEC to fabricate a sustainable self-cooling frame for cooling chip hotspots, which successfully cooled the hotspots at an acceptable temperature and reduced the unevenness of the chip’s temperature distribution [46]. Li et al. proposed a chip-on-TEC for active thermal management of high-power light-emitting diodes (LED), and the study showed that at an operating current of 1.0 A, it not only reduced the chip temperature by 51% but also increased the light output power of the LED [47].

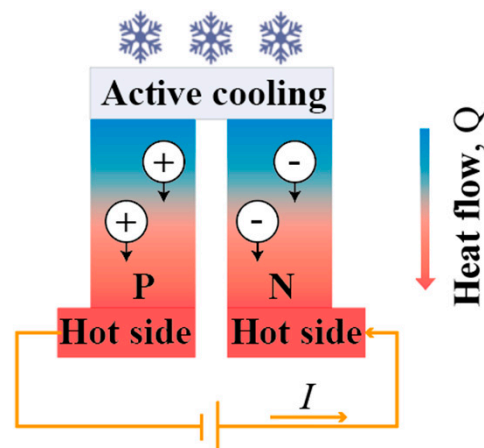


Figure 1. Principle of TEC.

In this work, we have utilized thermoelectric technology to cool the power devices in the control circuit of an air conditioner. This allowed us to accurately regulate the temperature of the power devices on the circuit board, which ensures that the air conditioner always runs efficiently [48–50]. To begin, we established a multi-physics field model with the help of COMSOL finite element analysis software [51–54]. Next, we compared the temperature field under conventional air-cooling with that after adding a TEC device. Finally, we analyzed the effect of the TEC operating current on the chip temperature. Our research findings present a novel solution for cooling the core components in air conditioners.

2. Simulations

Geometric modeling: The heat dissipation structure of the power device after adding the TEC is shown in Figure 2. To ensure the reliability of the power device in application, it is usually packaged with the upper part connected to the protective case through thermal interface material and the lower part connected to the PCB board through welding. The TEC is positioned at the lower end of the PCB to directly cool the chip, and the heat is dissipated through the air duct via the cooling fins under the TEC. An optical photo of the air conditioner circuit board is shown in Figure S1. This paper establishes geometric models for the two heat dissipation models of the chip, cooling through the cooling fins and the TEC combined with air-cooling, to study the effect of the TEC on the temperature control of the chip in this structure.

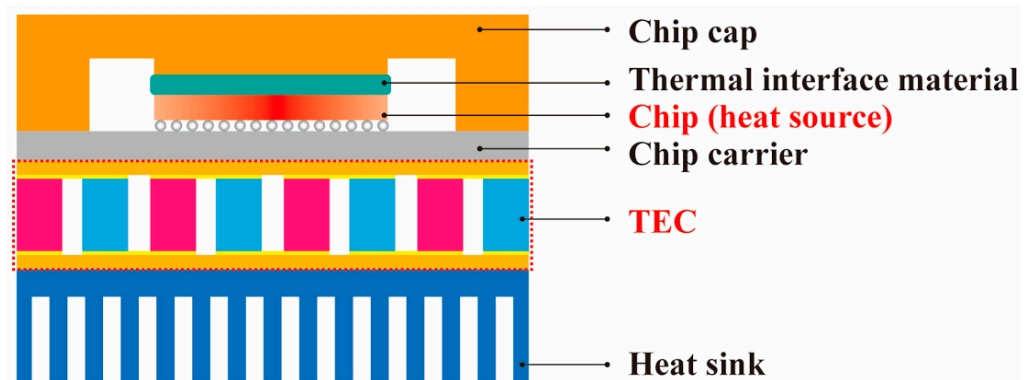


Figure 2. Heat dissipation structure for temperature control of power devices.

The TEC simulation model, as depicted in Figure 3, comprises a sandwich structure consisting of an upper ceramic substrate, upper electrodes, thermoelectric units, lower electrodes, and a lower ceramic substrate in a top-to-bottom configuration. The planar dimensions of the TEC measured $35 \times 57 \text{ mm}^2$, with a total vertical thickness of 3.8 mm, containing 416 thermoelectric legs measuring $1.4 \times 1.4 \times 1.6 \text{ mm}^3$ each, and the thicknesses of the ceramic substrate and the electrode were 0.8 mm and 0.3 mm, respectively. The CAD model and the geometric model of TEC forced cooling combined with fin air-cooling are shown in Figure S2 and Figure 4, and the model consists of power devices, TECs, heat-sink fins, and air ducts. The dimensions of the three core power devices were $35 \times 57 \times 3 \text{ mm}^3$, $20 \times 30 \times 3 \text{ mm}^3$, and $20 \times 30 \times 3 \text{ mm}^3$, corresponding to a power consumption of 173.81 W, 27.5 W, and 27.5 W, respectively, and an effective heat dissipation area of 1995 mm^2 , 587 mm^2 , and 587 mm^2 , respectively. The TEC featured the same planar dimensions as mentioned earlier, along with a flat fin size of $196 \times 210 \text{ mm}^2$, comprising 30 fins, and a center fin size of $52 \times 210 \times 1.5 \text{ mm}^3$. The air duct size was $430 \times 230 \times 86 \text{ mm}^3$. The contact interface between the TEC, the power device, and the fin was connected by a thermally conductive silicone grease with a thickness of 0.15 mm to ensure good contact heat conduction.

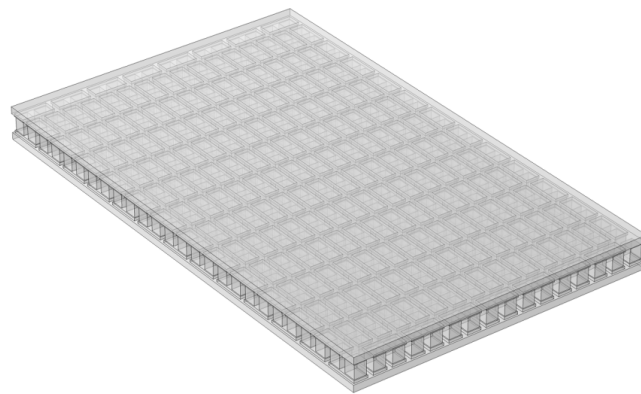


Figure 3. Simulation model of the TEC.

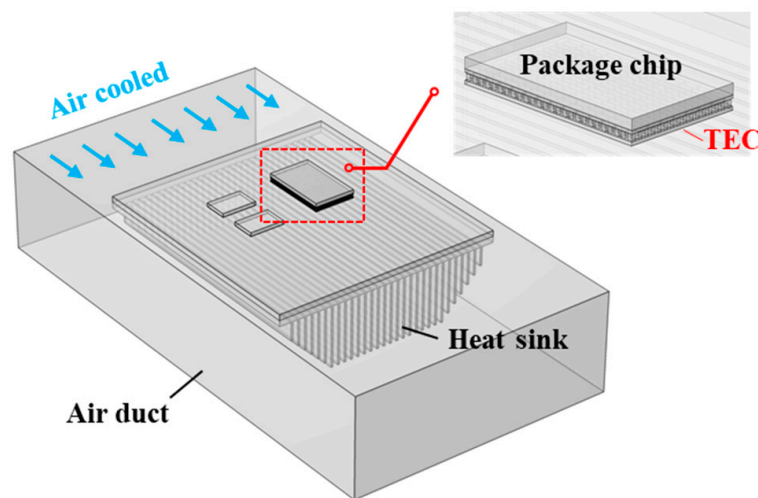


Figure 4. Fluid heat transfer simulation model of the TEC forced cooling combined with finned air-cooling.

Material property parameter setting: “FR4” from the material library of COMSOL Multiphysics 5.6 was used as the material of the circuit board, “6063 [solid]” alloy was used as the material of the heat-sink fin, and “air” was used as the material of the fluid heat transfer medium. The other materials in the model were custom materials and the specific material properties [55] are shown in Table 1.

Table 1. The main material property parameters of the simulation model.

Material	Parameter	Value
N-type $\text{Bi}_2\text{Se}_{0.3}\text{Te}_{2.7}$	Resistivity (10^4 S m^{-1})	7.640
	Thermal conductivity ($\text{W m}^{-1} \text{ K}^{-1}$)	1.275 (at room temperature)
P-type $\text{Bi}_{0.5}\text{Sb}_{1.5}\text{Te}_3$	Resistivity (10^4 S m^{-1})	9.535
	Thermal conductivity ($\text{W m}^{-1} \text{ K}^{-1}$)	1.362 (at room temperature)
Copper electrode	Resistivity (10^7 S m^{-1})	5.998
	Thermal conductivity ($\text{W m}^{-1} \text{ K}^{-1}$)	400
AlN substrate	Thermal conductivity ($\text{W m}^{-1} \text{ K}^{-1}$)	170
Thermal grease	Thermal conductivity ($\text{W m}^{-1} \text{ K}^{-1}$)	10

Multi-physical field setting: We invoked four physical field modules in COMSOL Multiphysics 5.6 for coupling solid and fluid heat transfer, laminar flow, current, and thermoelectric effects. Then, we needed to define the initial conditions and boundary conditions to determine the heat generation and heat transfer of the simulation models.

Initial conditions: the initial test temperature of all components in the model was 298.15 K (25 °C), the ambient temperature was 319.15 K (46 °C), and the wind speed at the inlet of the duct was 1.5 m s⁻¹.

Boundary conditions: The heat source of the power device was set by the domain heat source model in COMSOL, and the generalized source heat densities were 29,040,935.672, 15,393,226.98, and 15,393,226.98 W m⁻³. The heat transfer coefficients of the contact surfaces between the heat-sink fins and the air medium in the air duct in the air-cooled region were calculated by the laminar flow model.

Natural convection heat dissipation between air, the power device, and the TEC can be described by Fourier's law convective heat transfer process using Equation (1):

$$Q = h(T_{ambient} - T) \quad (1)$$

where h is the convective heat transfer coefficient and $T_{ambient}$ is the ambient temperature.

Referring to the convective heat transfer coefficient calculation model provided in COMSOL, the convective heat transfer coefficients at different locations for different materials in the TEC structure can be divided into three categories: top surface, bottom surface, and side surface, which we will discuss separately below.

The convective heat transfer coefficient between the TEC substrate and the electrode top surface (h_{top}) can be calculated according to Equation (2):

$$h_{top} = \begin{cases} \frac{\kappa}{L} \cdot 0.54 Ra_L^{\frac{1}{4}} & \text{if } T > T_{ambient} \text{ and } 10^4 \leq Ra_L \leq 10^7 \\ \frac{\kappa}{L} \cdot 0.15 Ra_L^{\frac{1}{3}} & \text{if } T < T_{ambient} \text{ and } 10^7 \leq Ra_L \leq 10^{11} \\ \frac{\kappa}{L} \cdot 0.27 Ra_L^{\frac{1}{4}} & \text{if } T \leq T_{ambient} \text{ and } 10^5 \leq Ra_L \leq 10^{10} \end{cases} \quad (2)$$

In the above equation, κ is the thermal conductivity of the heat transfer medium (air), L is the characteristic length (defined as the area/perimeter of the contact surface), and Ra_L is the Rayleigh number.

The heat transfer coefficient of the TEC bottom surface (h_{bot}) can be calculated the same as the TEC top surface (h_{top}).

The heat transfer coefficient (h_{side}) of the side of the TEC can be calculated according to Equation (3):

$$h_{side} = \begin{cases} \frac{\kappa}{H} \left(0.68 + \frac{0.67 Ra_L^{1/4}}{\left(1 + \left(\frac{0.492}{\mu C_p}\right)^{4/9}\right)} \right) & \text{if } Ra_L \leq 10^9 \\ \frac{\kappa}{H} \left(0.825 + \frac{0.387 Ra_L^{1/6}}{\left(1 + \left(\frac{0.492}{\mu C_p}\right)^{8/27}\right)} \right) & \text{if } Ra_L > 10^9 \end{cases} \quad (3)$$

where μ and C_p are the dynamic viscosity and heat capacity of air at qualitative temperature T_q , respectively. T_q is defined as $(T_{side} + T_{ambient})/2$.

The above sets of equations allowed us to accurately describe the convective heat transfer coefficients at different locations of the TEC in the simulation model, making the simulation results closer to the actual situation.

To simplify the model and reduce the amount of calculation, the following reasonable assumptions are proposed:

- (1) Only heat convection and heat exchange are considered, and the influence of heat radiation is not considered.

- (2) The surface of the cooling fin is regarded as an ideal plane, regardless of the influence of surface roughness on the air viscous heat transfer coefficient.
- (3) The contact interface between the cooling fin and the TEC is simplified, and a thermally conductive silicone grease layer is used as a substitute.

Finite element network division: The division technique of the finite element network is to divide each domain into smaller-sized subdomains of various shapes, and these subdomains are called finite elements. The more nodes of the primitive, the smaller the calculation error, and the tiny parts can also be reflected, and the longer the calculation time is, too. Reasonable grid division can obtain more accurate calculation results. In this paper, triangles were used to divide the mesh unit, and the division results are shown in Figures 5 and 6. In this model, 196,169 fixed points were selected and there were 821,207 cells with an average cell mass of 0.65.

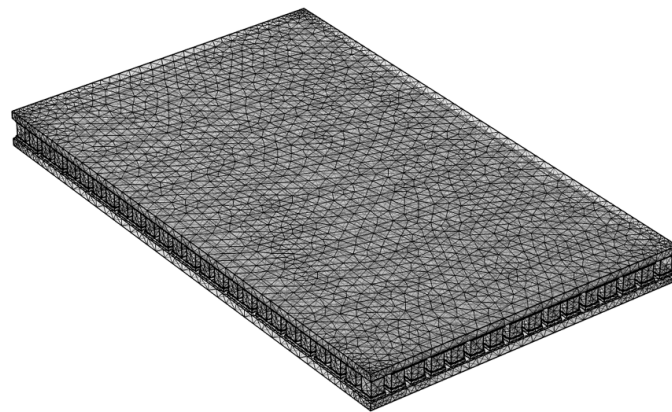


Figure 5. Finite element network division of the TEC.

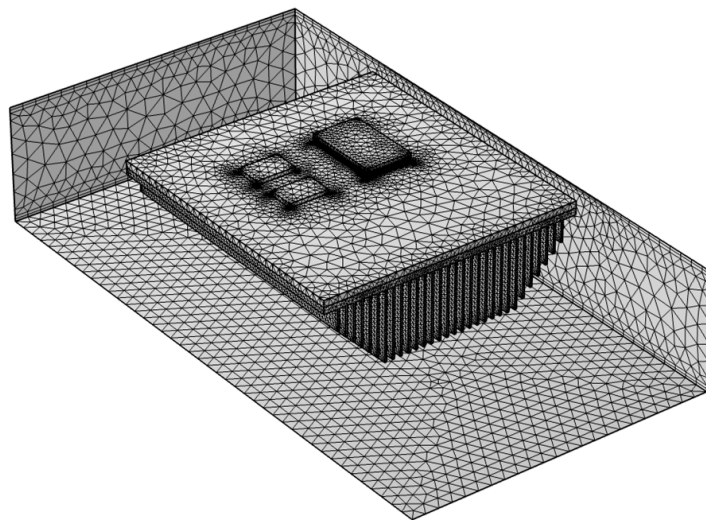


Figure 6. Finite element network division of the total system.

3. Results and Discussion

Firstly, we simulated the temperature distribution of the system with three power devices, generating 173.8 W, 27.5 W, and 27.5 W of heat at 319.15 K, respectively, only through air-cooling with the heat-sink fins and the air duct. When the air speed at the duct inlet was 1.5 ms^{-1} , the airflow velocity distribution in the duct was as shown in Figure 7. The air flow velocity at the fin surface was close to the airflow velocity at the inlet, and the streamlined fin configuration effectively reduced the effect of air-sticking resistance on the heat transfer coefficient at the fin surface.

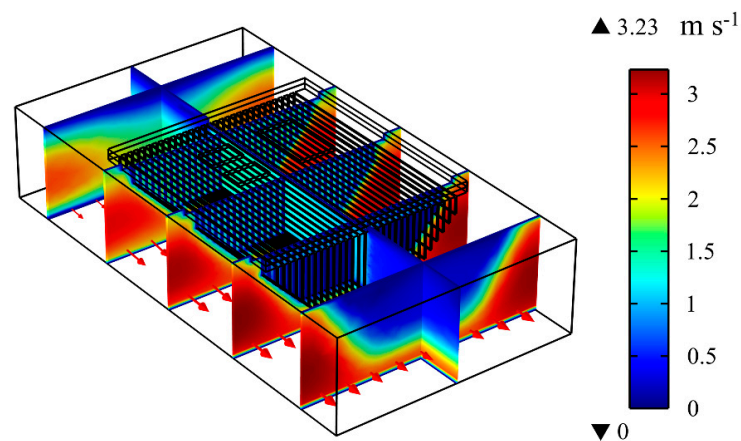


Figure 7. Airflow velocity distribution in the air duct.

Figure 8 illustrates the steady-state temperature distribution of different components in the system under convective air-cooling, and the whole process lasted about five minutes, as shown in Figure S3. As can be seen from Figure 8a, the power device had the highest temperature distribution among all system components, followed by the heat-sink fin and the air duct. Obviously, the heat was mainly concentrated on the power devices. The surface temperature of the power devices is proportional to their heat generation, and the heat-sink fins cannot effectively reduce the power device temperature. From Figure 8b,c, we can see that the maximum temperature of the high-heat-generating power device was 394.4 K, and the average temperature was 373.9 K, which exceeded its rated operating temperature of 368.1 K, while the maximum temperature of the low-power device was 371.6 K, and the average temperature was 358.2 K. Figure 8d shows the surface temperature distribution of the heat-sink fins. The temperature difference between the contact position of the power device and the heat-sink fins was not significant, which indicates that the uniform temperature performance of the heat-sink fins can meet the heat generation of the power device, so that most of the heat is transferred to the air through the heat-sink fins. The maximum surface temperature of the heat-sink fin was 363.8 K, and the average temperature was 348.5 K.

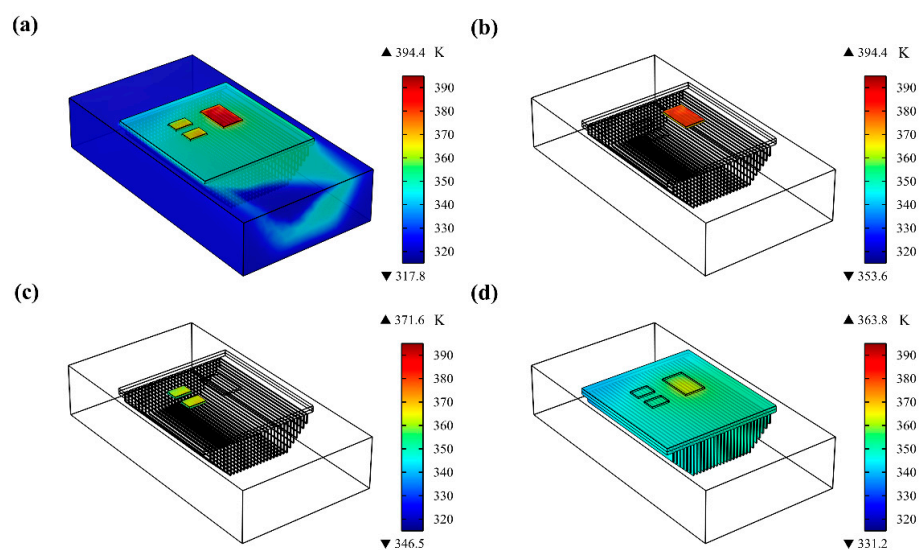


Figure 8. Steady-state temperature distribution under air-cooling: (a) the overall system, (b) the high-power-consumption power devices, (c) the low-power-consumption power devices, and (d) the heat-sink fins.

Then, we added a TEC beneath the power device that generates high levels of heat. The heat generated by the power device was actively carried to the heat-sink fins through the heat pump effect of the TEC. Consequently, the power device was temperature-controlled by active TEC cooling combined with the passive heat dissipation of the heat-sink fins. When the TEC operating current was 7.5 A, the steady-state temperature distribution of each component of the system was as shown in Figure 9, and the whole process lasted about eight minutes, as shown in Figure S4.

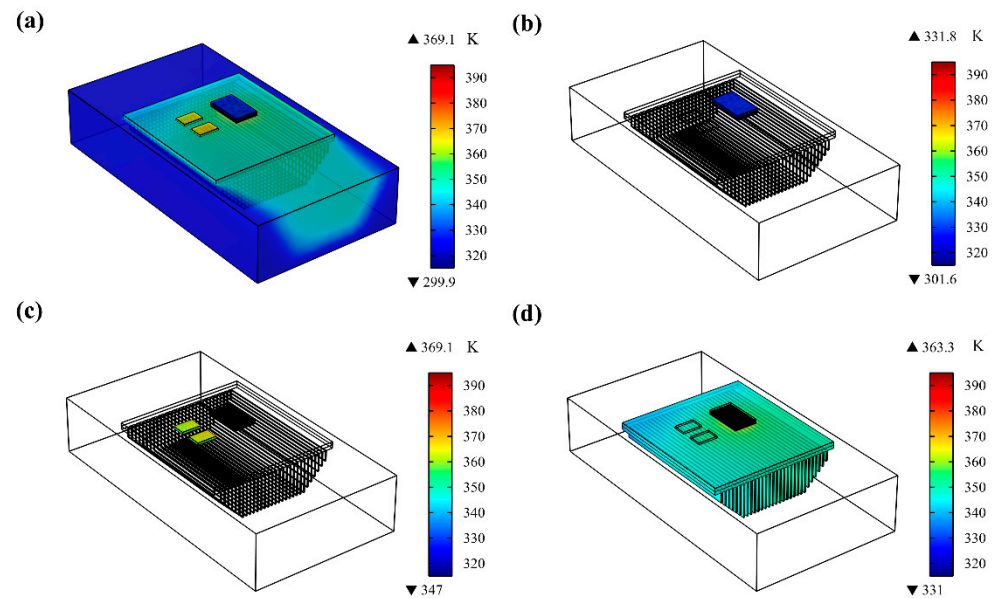


Figure 9. Steady-state temperature distribution under TEC forced cooling and air-cooling: (a) the overall system, (b) the high-power-consumption power devices, (c) the low-power-consumption power devices, and (d) the heat-sink fins.

As can be seen from Figure 9a, the combination of TEC active cooling with passive fin cooling resulted in a temperature distribution of each component in the system from high to low, namely the low-power devices without the TEC, the heat-sink fin, the air duct, and the high-power device with the TEC. The temperature distribution of the parts without the TEC was basically the same as that under single air-cooling, but the temperature of the high-power-consumption power device with the TEC was significantly lower. Additionally, the air temperature in the air duct was also different from that in the air-cooled heat sink because more heat was transferred to the air through convection heat transfer, causing the air temperature to become higher.

The high-power-consumption power device had a maximum temperature of 331.8 K and an average temperature of 326.5 K (Figure 9b). The addition of the TEC resulted in a significant reduction in temperature, with the maximum temperature dropping by 62.6 K and the average temperature dropping by 47.4 K compared to single air-cooling, which demonstrates that TEC active cooling has a significant effect on the temperature field of the power device. In contrast, the maximum and average temperatures of the low-power-consumption power device were 369.1 K and 358.8 K, respectively (Figure 9c). The addition of the TEC resulted in a lower maximum temperature, but a higher average temperature compared to the air-cooling mode. This indicates that the TEC actively transports the heat from the high-power-consumption power device to the heat-sink fins, and then the heat is transferred to the low-power-consumption power device through the heat-sink fins.

The temperature distribution on the heat-sink fins was basically the same as that under single air-cooling, with the maximum temperature of the heat-sink fins dropping from 363.8 K to 363.3 K and the average temperature rising from 348.5 K to 348.6 K (Figure 9d). The above simulation results demonstrate that the temperature of the power device was

well-controlled after the addition of the TEC, which is crucial for optimizing performance and extending the service life of these devices.

The previous research proved that the addition of the TEC under a constant operating current can effectively control the temperature of power devices. To further explore the reliability of TEC temperature control, the effect of the TEC on the operating temperature of power devices under different operating currents was experimentally studied. We systematically simulated the temperature field of the system under different TEC working currents. The average temperature of the high-power-consumption power device, low-power-consumption power device, and the heat-sink fins in the system varied with the working current of the TEC, as shown in Figure 10. It is evident that when the working current of the TEC was less than 5 A, the TEC had no active cooling effect on the power devices, even if the temperature was higher than that under air-cooling. This is because the cooling capacity of the TEC is related to the working current, and the TEC itself can also be regarded as a thermal resistance, of which the resistance varies with the working current in the heat transfer path. When the active cooling capacity minus the Joule heat is less than the original thermal conductivity, the thermal resistance effect will be realized. From the simulation results, the minimum working current of the TEC to achieve a cooling effect should reach 5 A under this working condition. When the working current of the TEC is further increased to 7.5 A and 10 A, the temperature of the cooled high-power-consumption power device can be further reduced to 326.5 K and 292.9 K, respectively, resulting in a significant improvement in temperature control. At the same time, the nearby low-power-consumption power devices and heat-sink fins will heat up because of the heat pump effect of the TEC, and the increase of the temperature of the heat-sink fins will also help to improve the air-cooled heat transfer.

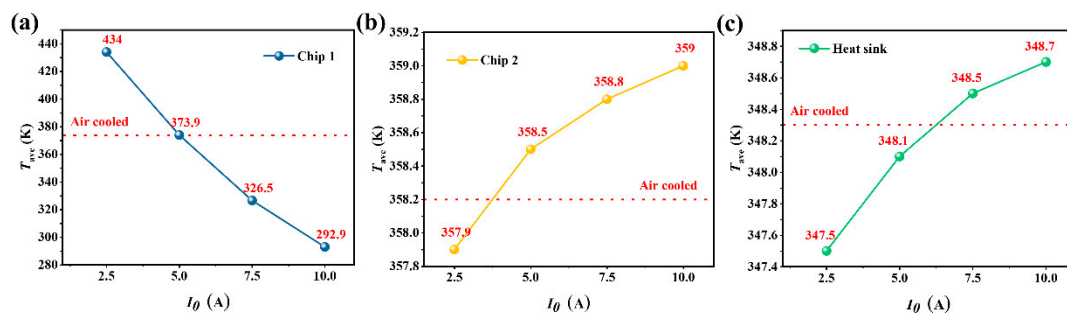


Figure 10. Influence of the TEC working current on the average temperature of: (a) the high-power-consumption power devices, (b) the low-power-consumption power devices, and (c) the heat-sink fins.

4. Conclusions

This work explored the active heat dissipation of thermoelectric cooling (TEC) for power devices in air conditioners through COMSOL finite element simulations. The simulation results revealed that in the single air-cooling mode, the maximum temperature of the power device with 173.8 W power consumption reached 394.4 K, and the average temperature reached 373.9 K, which exceeded its rated operating temperature of 368.1 K. However, after incorporating the TEC, the maximum temperature of the power device decreased to 331.8 K at an operating current of 7.5 A, and the average temperature of the device was reduced to 326.5 K. This demonstrated that TEC active cooling had a significant effect on the temperature control of the power device, reducing the maximum and average temperatures by 62.6 K and 47.4 K, respectively, compared to single air-cooling. Furthermore, we examined the effect of the TEC operating current on the temperature control effect of the power device, revealing a minimum TEC operating current of 5 A. In short, the research results showed that thermoelectric cooling technology can be well-used in the power devices in the air conditioner control circuit to prevent the reduction of the air-conditioning cooling efficiency caused by overheating of the power devices theoretically.

It can not only precisely adjust the temperature of the power devices on the circuit board to ensure that the air conditioner always operates in a high-efficiency mode but can also minimize the energy consumption and reduce emissions.

Supplementary Materials: The following supporting information can be downloaded at: <https://www.mdpi.com/article/10.3390/app13127274/s1>, Figure S1: The optical photo of air conditioner circuit board; Figure S2: The CAD model of cooling system; Figure S3: Temperature distribution of the system without TEC cooling at different times; Figure S4: Temperature distribution of the system with TEC cooling at different times.

Author Contributions: D.Y. and Y.Y. conceived the project; J.W., K.T. and Y.X. (Yubing Xing) carried out the finite element simulation; D.Y., J.W., K.H., Y.X. (Yani Xiao), Y.L. and Y.Y. analyzed the data; J.W., K.H. and D.Y. co-wrote the manuscript. All authors have read and agreed to the published version of the manuscript.

Funding: This work was financially supported by the National Natural Science Foundation of China (52202289), the International Postdoctoral Exchange Fellowship Program (PC2022044), and the National Key Research and Development Program of China (2019YFA0704900).

Institutional Review Board Statement: Not applicable.

Informed Consent Statement: Not applicable.

Data Availability Statement: Not applicable.

Conflicts of Interest: The authors declare no conflict of interest.

References

1. Puttaswamy, K.; Loh, G.H. Thermal Analysis of a 3D Die-Stacked High-Performance Microprocessor. In Proceedings of the 16th ACM Great Lakes Symposium on VLSI, Philadelphia, PA, USA, 30 April–1 May 2006; pp. 19–24.
2. Nada, S.; Alshaer, W. Comprehensive Parametric Study of Using Carbon Foam Structures Saturated with PCMs in Thermal Management of Electronic Systems. *Energy Convers. Manag.* **2015**, *105*, 93–102. [[CrossRef](#)]
3. Mathew, J.; Krishnan, S. A Review on Transient Thermal Management of Electronic Devices. *J. Electron. Packag.* **2022**, *144*, 010801. [[CrossRef](#)]
4. Brooks, D.; Martonosi, M. Dynamic Thermal Management for High-Performance Microprocessors. In Proceedings of the HPCA Seventh International Symposium on High-Performance Computer Architecture, Monterrey, Mexico, 19–24 January 2001; IEEE: Piscataway, NJ, USA, 2001; pp. 171–182.
5. Haywood, A.M.; Sherbeck, J.; Phelan, P.; Varsamopoulos, G.; Gupta, S.K. The Relationship among CPU Utilization, Temperature, and Thermal Power for Waste Heat Utilization. *Energy Convers. Manag.* **2015**, *95*, 297–303. [[CrossRef](#)]
6. Yi, J.; Liu, W.; Jiang, W.; Qin, M.; Yang, L.; Liu, D.; Xiao, C.; Du, L.; Sha, E.H.-M. An Improved Thermal Model for Static Optimization of Application Mapping and Scheduling in Multiprocessor System-on-Chip. In Proceedings of the 2014 IEEE Computer Society Annual Symposium on VLSI, Tampa, FL, USA, 9–11 July 2014; IEEE: Piscataway, NJ, USA, 2014; pp. 547–552.
7. Subramanian, V.; Ramesh, P.K.; Somani, A.K. Managing the Impact of On-Chip Temperature on the Lifetime Reliability of Reliably Overclocked Systems. In Proceedings of the 2009 Second International Conference on Dependability, Athens, Greece, 18–23 June 2009; IEEE: Piscataway, NJ, USA, 2009; pp. 156–161.
8. Prakash, A.; Amrouch, H.; Shafique, M.; Mitra, T.; Henkel, J. Improving Mobile Gaming Performance through Cooperative CPU-GPU Thermal Management. In Proceedings of the 53rd Annual Design Automation Conference, Austin, TX, USA, 5–9 June 2016; pp. 1–6.
9. Hager, G.; Treibig, J.; Habich, J.; Wellein, G. Exploring Performance and Power Properties of Modern Multi-Core Chips via Simple Machine Models. *Concurr. Comput. Pract. Exp.* **2016**, *28*, 189–210. [[CrossRef](#)]
10. Garimella, S.V.; Yeh, L.-T.; Persoons, T. Thermal Management Challenges in Telecommunication Systems and Data Centers. *IEEE Trans. Compon. Packag. Manuf. Technol.* **2012**, *2*, 1307–1316. [[CrossRef](#)]
11. Suszko, A.; El-Genk, M.S. Thermally Anisotropic Composite Heat Spreaders for Enhanced Thermal Management of High-Performance Microprocessors. *Int. J. Therm. Sci.* **2016**, *100*, 213–228. [[CrossRef](#)]
12. Kong, J.; Chung, S.W.; Skadron, K. Recent Thermal Management Techniques for Microprocessors. *ACM Comput. Surv. (CSUR)* **2012**, *44*, 1–42. [[CrossRef](#)]
13. Li, Y.; Gong, L.; Ding, B.; Xu, M.; Joshi, Y. Thermal Management of Power Electronics with Liquid Cooled Metal Foam Heat Sink. *Int. J. Therm. Sci.* **2021**, *163*, 106796. [[CrossRef](#)]
14. Laloya, E.; Lucia, O.; Sarnago, H.; Burdío, J.M. Heat Management in Power Converters: From State of the Art to Future Ultrahigh Efficiency Systems. *IEEE Trans. Power Electron.* **2015**, *31*, 7896–7908. [[CrossRef](#)]

15. Shatikian, V.; Ziskind, G.; Letan, R. Numerical Investigation of a PCM-Based Heat Sink with Internal Fins. *Int. J. Heat Mass Transf.* **2005**, *48*, 3689–3706. [[CrossRef](#)]
16. Lee, Y.J.; Singh, P.K.; Lee, P.S. Fluid Flow and Heat Transfer Investigations on Enhanced Microchannel Heat Sink Using Oblique Fins with Parametric Study. *Int. J. Heat Mass Transf.* **2015**, *81*, 325–336. [[CrossRef](#)]
17. Qi, Z. Advances on Air Conditioning and Heat Pump System in Electric Vehicles—A Review. *Renew. Sustain. Energy Rev.* **2014**, *38*, 754–764. [[CrossRef](#)]
18. Jin, X.; Ma, E.W.; Cheng, L.L.; Pecht, M. Health Monitoring of Cooling Fans Based on Mahalanobis Distance with MRMR Feature Selection. *IEEE Trans. Instrum. Meas.* **2012**, *61*, 2222–2229. [[CrossRef](#)]
19. Leroy, A.; Bhatia, B.; Kelsall, C.C.; Castillejo-Cuberos, A.; Di Capua, H.M.; Zhao, L.; Zhang, L.; Guzman, A.; Wang, E. High-Performance Subambient Radiative Cooling Enabled by Optically Selective and Thermally Insulating Polyethylene Aerogel. *Sci. Adv.* **2019**, *5*, eaat9480. [[CrossRef](#)] [[PubMed](#)]
20. Xiang, X.; Yang, J.; Fan, A.; Liu, W. A Comparison between Cooling Performances of Water-Based and Gallium-Based Micro-Channel Heat Sinks with the Same Dimensions. *Appl. Therm. Eng.* **2018**, *137*, 1–10. [[CrossRef](#)]
21. Khan, Y.; Sarowar, M.T.; Mobarrat, M.; Rahman, M.H. Performance Comparison of a Microchannel Heat Sink Using Different Nano-Liquid Metal Fluid Coolant: A Numerical Study. *J. Therm. Sci. Eng. Appl.* **2022**, *14*, 091014. [[CrossRef](#)]
22. Muhammad, A.; Selvakumar, D.; Iranzo, A.; Sultan, Q.; Wu, J. Comparison of Pressure Drop and Heat Transfer Performance for Liquid Metal Cooled Mini-Channel with Different Coolants and Heat Sink Materials. *J. Therm. Anal. Calorim.* **2020**, *141*, 289–300. [[CrossRef](#)]
23. Tan, F.; Tso, C. Cooling of Mobile Electronic Devices Using Phase Change Materials. *Appl. Therm. Eng.* **2004**, *24*, 159–169. [[CrossRef](#)]
24. Li, W.; Wang, F.; Cheng, W.; Chen, X.; Zhao, Q. Study of Using Enhanced Heat-Transfer Flexible Phase Change Material Film in Thermal Management of Compact Electronic Device. *Energy Convers. Manag.* **2020**, *210*, 112680. [[CrossRef](#)]
25. Zhou, Z.; Zhao, Y.; Ling, Z.; Zhang, Z.; Lin, W.; Fang, X. Simulative Study on the Performance of Polymeric Composites Containing Phase Change Capsules for Chip Heat Dissipation. *J. Energy Storage* **2023**, *68*, 107851. [[CrossRef](#)]
26. Faraji, M.; El Qarnia, H.; Lakhal, E.K. Thermal Analysis of a Phase Change Material Based Heat Sink for Cooling Protruding Electronic Chips. *J. Therm. Sci.* **2009**, *18*, 268–275. [[CrossRef](#)]
27. Zhao, Y.; Zhang, Z.; Cai, C.; Zhou, Z.; Ling, Z.; Fang, X. Vertically Aligned Carbon Fibers-Penetrated Phase Change Thermal Interface Materials with High Thermal Conductivity for Chip Heat Dissipation. *Appl. Therm. Eng.* **2023**, *230*, 120807. [[CrossRef](#)]
28. Tang, H.; Tang, Y.; Wan, Z.; Li, J.; Yuan, W.; Lu, L.; Li, Y.; Tang, K. Review of Applications and Developments of Ultra-Thin Micro Heat Pipes for Electronic Cooling. *Appl. Energy* **2018**, *223*, 383–400. [[CrossRef](#)]
29. Zhu, L.; Tan, H.; Yu, J. Analysis on Optimal Heat Exchanger Size of Thermoelectric Cooler for Electronic Cooling Applications. *Energy Convers. Manag.* **2013**, *76*, 685–690. [[CrossRef](#)]
30. Byon, C. Heat Pipe and Phase Change Heat Transfer Technologies for Electronics Cooling. In *Electronics Cooling*; IntechOpen: Rijeka, Croatia, 2016. [[CrossRef](#)]
31. Groll, M.; Schneider, M.; Sartre, V.; Zaghdoudi, M.C.; Lallemant, M. Thermal Control of Electronic Equipment by Heat Pipes. *Rev. Générale Therm.* **1998**, *37*, 323–352. [[CrossRef](#)]
32. Abdelkareem, M.A.; Maghrabie, H.M.; Sayed, E.T.; Kais, E.-C.A.; Abo-Khalil, A.G.; Al Radi, M.; Baroutaji, A.; Olabi, A. Heat Pipe-Based Waste Heat Recovery Systems: Background and Applications. *Therm. Sci. Eng. Prog.* **2022**, *29*, 101221. [[CrossRef](#)]
33. Baby, R.; Balaji, C. Thermal Management of Electronics Using Phase Change Material Based Pin Fin Heat Sinks. *J. Phys. Conf. Ser.* **2012**, *395*, 012134. [[CrossRef](#)]
34. Goharshadi, E.; Ahmadzadeh, H.; Samiee, S.; Hadadian, M. Nanofluids for Heat Transfer Enhancement—A Review. *Phys. Chem. Res.* **2013**, *1*, 1–33.
35. Zhao, D.; Tan, G. A Review of Thermoelectric Cooling: Materials, Modeling and Applications. *Appl. Therm. Eng.* **2014**, *66*, 15–24. [[CrossRef](#)]
36. Enescu, D.; Virjoghe, E.O. A Review on Thermoelectric Cooling Parameters and Performance. *Renew. Sustain. Energy Rev.* **2014**, *38*, 903–916. [[CrossRef](#)]
37. Chen, W.; Shi, X.; Zou, J.; Chen, Z. Thermoelectric Coolers: Progress, Challenges, and Opportunities. *Small Methods* **2022**, *6*, 2101235. [[CrossRef](#)]
38. Pourkiaei, S.M.; Ahmadi, M.H.; Sadeghzadeh, M.; Moosavi, S.; Pourfayaz, F.; Chen, L.; Yazdi, M.A.P.; Kumar, R. Thermoelectric Cooler and Thermoelectric Generator Devices: A Review of Present and Potential Applications, Modeling and Materials. *Energy* **2019**, *186*, 115849. [[CrossRef](#)]
39. Bansal, P.; Martin, A. Comparative Study of Vapour Compression, Thermoelectric and Absorption Refrigerators. *Int. J. Energy Res.* **2000**, *24*, 93–107. [[CrossRef](#)]
40. Liang, K.; Li, Z.; Chen, M.; Jiang, H. Comparisons between Heat Pipe, Thermoelectric System, and Vapour Compression Refrigeration System for Electronics Cooling. *Appl. Therm. Eng.* **2019**, *146*, 260–267. [[CrossRef](#)]
41. Chougule, S.S.; Sahu, S. Thermal Performance of Nanofluid Charged Heat Pipe with Phase Change Material for Electronics Cooling. *J. Electron. Packag.* **2015**, *137*, 021004. [[CrossRef](#)]
42. Singh, V.; Sisodia, S.; Patel, A.; Shah, T.; Das, P.; Patel, R.; Bhavsar, R. Thermoelectric Cooler (TEC) Based Thermal Control System for Space Applications: Numerical Study. *Appl. Therm. Eng.* **2023**, *224*, 120101. [[CrossRef](#)]

43. Gillott, M.; Jiang, L.; Riffat, S. An Investigation of Thermoelectric Cooling Devices for Small-Scale Space Conditioning Applications in Buildings. *Int. J. Energy Res.* **2010**, *34*, 776–786. [[CrossRef](#)]
44. Chen, W.-Y.; Shi, X.-L.; Zou, J.; Chen, Z.-G. Thermoelectric Coolers for On-Chip Thermal Management: Materials, Design, and Optimization. *Mater. Sci. Eng. R Rep.* **2022**, *151*, 100700. [[CrossRef](#)]
45. Moazzez, A.F.; Najafi, G.; Ghobadian, B.; Hoseini, S.S. Numerical Simulation and Experimental Investigation of Air Cooling System Using Thermoelectric Cooling System. *J. Therm. Anal. Calorim.* **2020**, *139*, 2553–2563. [[CrossRef](#)]
46. Al-Shehri, S.A. Cooling Computer Chips with Cascaded and Non-Cascaded Thermoelectric Devices. *Arab. J. Sci. Eng.* **2019**, *44*, 9105–9126. [[CrossRef](#)]
47. Li, S.; Liu, J.; Ding, L.; Liu, J.; Xu, J.; Peng, Y.; Chen, M. Active Thermal Management of High-Power LED through Chip on Thermoelectric Cooler. *IEEE Trans. Electron Devices* **2021**, *68*, 1753–1756. [[CrossRef](#)]
48. Lou, L.; Shou, D.; Park, H.; Zhao, D.; Wu, Y.S.; Hui, X.; Yang, R.; Kan, E.C.; Fan, J. Thermoelectric Air Conditioning Undergarment for Personal Thermal Management and HVAC Energy Saving. *Energy Build.* **2020**, *226*, 110374. [[CrossRef](#)]
49. Sasidharan, M.; Mohd Sabri, M.F.; Wan Muhammad Hatta, S.F.; Ibrahim, S. A Review on the Progress and Development of Thermoelectric Air Conditioning System. *Int. J. Green Energy* **2023**, *20*, 1–17. [[CrossRef](#)]
50. Said, M.; Hassan, H. Impact of Energy Storage of New Hybrid System of Phase Change Materials Combined with Air-Conditioner on Its Heating and Cooling Performance. *J. Energy Storage* **2021**, *36*, 102400. [[CrossRef](#)]
51. Ma, K.; Zuo, Z.; Wang, W. Design and Experimental Study of an Outdoor Portable Thermoelectric Air-Conditioning System. *Appl. Therm. Eng.* **2023**, *219*, 119471. [[CrossRef](#)]
52. Seyednezhad, M.; Najafi, H. Numerical Analysis and Parametric Study of a Thermoelectric-Based Radiant Ceiling Panel for Building Cooling Applications. In Proceedings of the ASME International Mechanical Engineering Congress and Exposition, Virtual Online, 16–19 November 2020; American Society of Mechanical Engineers: New York, NY, USA, 2020; Volume 84560, p. V008T08A030.
53. Manikandan, S.; Selvam, C.; Pavan Sai Praful, P.; Lamba, R.; Kaushik, S.; Zhao, D.; Yang, R. A Novel Technique to Enhance Thermal Performance of a Thermoelectric Cooler Using Phase-Change Materials. *J. Therm. Anal. Calorim.* **2020**, *140*, 1003–1014. [[CrossRef](#)]
54. Venkatesan, K.; Venkataramanan, M. Experimental and Simulation Studies on Thermoelectric Cooler: A Performance Study Approach. *Int. J. Thermophys.* **2020**, *41*, 1–23. [[CrossRef](#)]
55. Hu, K.; Yang, D.; Hui, Y.; Zhang, H.; Song, R.; Liu, Y.; Wang, J.; Wen, P.; He, D.; Liu, X.; et al. Optimized Thermal Design for Excellent Wearable Thermoelectric Generator. *J. Mater. Chem. A* **2022**, *10*, 24985–24994. [[CrossRef](#)]

Disclaimer/Publisher’s Note: The statements, opinions and data contained in all publications are solely those of the individual author(s) and contributor(s) and not of MDPI and/or the editor(s). MDPI and/or the editor(s) disclaim responsibility for any injury to people or property resulting from any ideas, methods, instructions or products referred to in the content.